Ecotoxicology and Environmental Safety 172 (2019) 1–10

Contents lists available at ScienceDirect

Ecotoxicology and Environmental Safety

journal homepage: www.elsevier.com/locate/ecoenv

Metabolic and proteomic mechanism of benzo[a]pyrene degradation by *Brevibacillus brevis*

Yueping Zhu[a], Kaiyun Chen[b], Yingqi Ding[c], Donglin Situ[c], Yi Li[c], Yan Long[c], Lili Wang[c], Jinshao Ye[c,*]

[a] Technology Research Center for Petrochemical Resources Clean Utilization of Guangdong Province, Faculty of Environmental Science and Engineering, Guangdong University of Petrochemical Technology, Maoming 525000, Guangdong, China
[b] Child Developmental-Behavioral Center, The Third Affiliated Hospital of Sun Yat-sen University, Guangzhou 510630, China
[c] Guangdong Key Laboratory of Environmental Pollution and Health, School of Environment, Jinan University, Guangzhou 510632, Guangdong, China

ARTICLE INFO

Keywords:
Benzo[a]pyrene
Biodegradation
Proteomics
Ion
Enzyme

ABSTRACT

Benzo[a]pyrene (BaP) is a model compound of polycyclic aromatic hydrocarbons. The relationship between its toxicity and some target biomolecules has been investigated. To reveal the interactions of BaP biodegradation and metabolic network, BaP intermediates, proteome, carbon metabolism and ion transport were analyzed. The results show that 76% BaP was degraded by *Brevibacillus brevis* within 7 d through the cleavage of aromatic rings with the production of 1-naphthol and 2-naphthol. During this process, the expression of xylose isomerase was induced for xylose metabolism, whereas, α-cyclodextrin could no longer be metabolized. Lactic acid, acetic acid and oxalic acid at 0.1–1.2 mg dm^{-3} were released stemming from their enhanced biosynthesis in the pathways of pyruvate metabolism and citrate cycle, while 5–7 mg dm^{-3} of PO_4^{3-} were transported for energy metabolism. The relative abundance of 43 proteins was significantly increased for pyruvate metabolism, citrate cycle, amino acid metabolism, purine metabolism, ribosome metabolism and protein synthesis.

1. Introduction

Brevibacillus brevis is a Gram-positive and spore-forming bacterium secreting some functional metabolites with a broad-spectrum antibiotic activity (Pawlowski et al., 2016; Song et al., 2012). It is capable of transforming some hazardous pollutants with aromatic rings, including poly brominated diphenyl ethers (Tang et al., 2014), organotins (Ye et al., 2013), pyrene (Liao et al., 2015; Wei et al., 2017) and poly vinyl alcohol (Kim and Yoon, 2010), to nontoxic intermediates because *B. brevis* can express enzymes catalyzing the cleavage of the C–C bands in aromatic rings. During the degradation process, proteins related to aromatic compound transport, energy generation, amino acid metabolism were significantly differentially expressed (Wei et al., 2017). These findings indicate that *B. brevis* might be an effective strain for the degradation of polycyclic aromatic hydrocarbons.

Because of its accumulative, cytotoxic, mutagenic and carcinogenic properties, benzo[a]pyrene (BaP) is a model compound and one of the most discussed members of polycyclic aromatic hydrocarbons (Chen et al., 2018; Fanali et al., 2018). Some studies at molecular level have found that BaP could induce the expression of cytochrome P450s (Kim et al., 2013; Speciale et al., 2018). They could combine with epoxide hydrolase converting BaP to carcinogen benzo[a]pyrene-7, 8-diol-9, 10-epoxide. To prevent the damage triggered by BaP, cells would enhance the expression of glutathione-S-transferases, UDP-glucuronosyl transferases and sulfotransferases for the detoxification of BaP and its intermediates through conjugation reactions (Shi et al., 2017). During this process, the synthesis of some proteins, namely heat shock proteins and arginine kinase, would also be altered (Krais et al., 2016; Zhang et al., 2017).

For the biodegradation, benzo[a]pyrene-1, 6-quinone, 1-hydroxy-2-benzoic acid, and benzoic acid have been identified as the metabolites of BaP degradation by white-rot fungus *Armillaria* sp. F022 (Hadibarata and Kristanti, 2012). Some differently abundant ABC transporters, S-layer protein and cysteine synthase associated with BaP transport by *Stenotrophomonas maltophilia* (Shuona et al., 2017), and 22 genes in *Altererythrobacter epoxidivorans* related to BaP degradation (Li et al., 2016) have been found. A putative DszA/NtaA-like monooxygenase and a NifH-like reductase were specifically induced under the exposure to BaP (Sowada et al., 2014). Cytochrome P4501A has been confirmed to be an enzyme catalyzed BaP through the degradation by an engineered *Shewanella oneidensis* expressed the recombinant P450 (Chang et al., 2014). All those findings have presented insights into the relationship

* Corresponding author.
E-mail addresses: folaye@126.com, jsye@jnu.edu.cn (J. Ye).

https://doi.org/10.1016/j.ecoenv.2019.01.044
Received 3 December 2018; Received in revised form 7 January 2019; Accepted 10 January 2019
Available online 18 January 2019
0147-6513/

between BaP biotransformation and some functional biomolecules.

To reveal the interactions of BaP biodegradation and cellular metabolic network, omics technologies will be the suitable approaches (Ye et al., 2017). For example, the isobaric tags for relative and absolutely quantitation (iTRAQ) proteomic technology is a high-throughput method that is used to identify, characterize and quantify proteome. Several studies have already focused on applying this approach for the screening of functional genes and proteins for pollutant biodegradation (Kjeldal et al., 2016; Li et al., 2018). To clarify the relationship between BaP biodegradation and cellular metabolic network, the expression of cellular proteome, the uptake and release of substrates and ions were investigated.

2. Materials and methods

2.1. Chemicals

BaP was purchased from Sigma Aldrich (St. Louis, MO, USA). The concentrations of beef extract, peptone, NaCl and $MgSO_4{\cdot}7H_2O$ in the culture medium were 3, 10 and 5 g dm^{-3} and 50 mg dm^{-3}, respectively. The treatment solution for BaP degradation contained (in mg dm^{-3}) 100 $Na_2HPO_4{\cdot}12H_2O$, 100 KH_2PO_4, 150 NaCl, 20 NH_4NO_3, 10 $MgSO_4{\cdot}7H_2O$, 1 $MnSO_4{\cdot}H_2O$, 1 $FeSO_4{\cdot}7H_2O$, 1 $CaCl_2{\cdot}2H_2O$ and 20 sucrose fatty acid ester.

2.2. Microbial culture

Brevibacillus brevis was isolated by our group from an e-waste dismantling area in Guiyu, Guangdong Province, China (Ye et al., 2013). It was inoculated into the culture medium at 30 °C on a rotary shaker at a rotation speed of 100 r min^{-1} for 24 h, followed by centrifugation at 3500*g* for 5 min. The separated cells were then rinsed three times with sterile treatment solution before used.

2.3. Benzo[a]pyrene removal, degradation and biosorption

The separated cells were used to prepare a cellular suspension by adding sterile treatment solution. Immediately, the suspension was added to 20 cm^3 of treatment solution with 1 mg dm^{-3} of BaP at the final biomass dosage of 0.3 g dm^{-3}. The removal and degradation of BaP in the above solution were performed in the dark shaking on a rotary shaker at a rotation speed of 100 r min^{-1}. Effects of pH values, temperature, degradation time and biomass dosages on BaP biosorption and degradation were assessed. In the experiments, the initial pH values of solutions were set at 3, 4, 5, 6, 7, 8, 9, 10 and 11. Degradation periods ranged from 2 h to 7 d. Temperature was set at 20, 25, 30, 35 and 40 °C, respectively, while biomass dosages were ranged from 0.05 to 3.00 g dm^{-3}. After treatment, the total residual BaP and its metabolites were analyzed to determine the degradation efficiency and mechanism. Cells in the parallel treatment solution were separated by centrifugation at 3500*g* for 5 min. Residual BaP, ions and organic acids in the resultant supernatant were detected to determine the removal efficiency, cellular transport and release.

To clarify the trend of BaP biosorption, cells separated from solution after BaP treatment were rinsed by the phosphate buffer solution for 20 min. Subsequently, BaP in the supernatant was detected to determine the BaP adsorption by cellular surface.

To reveal the contribution of metabolism-independent adsorption to BaP bio-removal, the separated cells from culture medium were inactivated by 2% glutaraldehyde for 24 h. After rinse three times with sterile treatment solution, 0.3 g dm^{-3} of these inactivated cells were used to absorb 1 mg dm^{-3} of BaP for 2 h to 7 d. After adsorption, the cells were separated by centrifugation at 3500*g*. The residual BaP in supernatant was detected to determine the adsorption efficiency.

The controls were run in parallel in flasks contained solutions without cells or BaP. Method blanks were prepared following the procedure of BaP degradation but starting with treatment solution that did not contain cells and BaP. All of the experiments were performed in triplicate. The significant difference analysis between the treated samples and the control samples was performed using a two-tailed unpaired student's *t*-test by GraphPad Prism 5.0. For statistical comparison, $p < 0.05$ was considered as significant.

2.4. Determination of benzo[a]pyrene and its metabolites

The analytical method was performed according to a reference (Chen et al., 2013). Briefly, GC–MS analysis was conducted by QP2010 (Shimadzu, Japan) using an Rxi-5MS GC column (30 m × 0.25 mm × 0.25 μm). Helium was used as the carrier gas with a constant flow of 1.50 cm^3 min^{-1}. The column temperature program started at 40 °C, held for 2 min, then the oven was heated to 110 °C at a rate of 35 °C min^{-1}, followed by an increase to 129 °C at 15 °C min^{-1} and continued to be heated to 270 °C with a rate of 20 °C min^{-1}, finally the temperature reached 280 °C and held for 5 min. The solvent cut time was set to 4 min. The GC–MS interface temperature was maintained at 250 °C. Mass spectra were recorded at 1 scan s^{-1} under electronic impact with electron energy of 70 eV, mass range 50–550 atom to mass unit. The temperature of ion source was set at 220.

The mean values were used in the calculations. The statistical analysis of BaP treatment was performed by SPSS version 13.0 using Pearson correlation tests. Pollutant compute properties were performed by Chembio office 2012.

2.5. Determination of organic acids and carbon substrate

After the BaP degradation by 0.3 g dm^{-3} cells for 0.5 h–10 d, the solutions were centrifuged at 3500*g* for 10 min. The resultant supernatant was filtered using a 0.22-μm polyether sulfone filter, and the concentrations of ions, oxalic acid, acetic acid and lactic acid were detected by an ICS-2500 ion chromatography system (Dionex, Sunnyvale, USA). The concentrations of these acids in treatment solutions without inoculation or BaP were also detected. Method blanks were prepared following the analysis procedure starting with water that was used to prepare treatment solution. All of the experiments were performed in triplicate. The alterations of ion concentration in the present experiment were measured as the experimental minus the control concentrations, so a negative value means ion use and a positive value implies ion release by *B. brevis*.

Biolog microplates were used to analyze the cellular activities in carbon nutrient metabolism after BaP degradation. Cells did not degrade BaP were used as the control. The 96-well microplates contain 31 kinds of carbon nutrients. Each three parallel sample wells hold liquid with one kind of carbon substrates. Three water wells were set as the control. In brief, cells after BaP degradation was diluted in a 0.85% sterilized saline solution 100 times followed by the inoculation of 150 mm^3 of the mixture into each well of microplates at 25 °C in the dark. The optical density at 590 nm of each well was determined every 12 h.

2.6. Protein preparation and digestion

After the BaP degradation for 1 d, cells were suspended in 1 cm^3 lysis buffer (15 mM Tris-HCl, 7 M urea, 2 M thiourea, 1% w/v dithiothreitol, 4% w/v 3-(3-Cholamidopropyl)-dimethylammonio propanesulfonate with 0.2 g dm^{-3} phenylmethylsulfonyl fluoride), 2% v/v IPG buffer and 0.6 g dm^{-3} dithiothreitol. After vibration for 10 s, samples were frozen in liquid nitrogen thrice for 15 min per time, followed by ultrasonication for 20 min. Subsequently, a nuclease mix was added to the lysate at a final concentration of 1% v/v. After the mixture was incubated at 4 °C for 30 min, the cell debris was removed at 4 °C by centrifugation at 13,500*g* for 1 h.

Proteins from each sample were reduced with 2 mm^3 of reducing

reagent at 37 °C for 1 h. The cysteines in proteins were blocked with 1 mm^3 of cystein-blocking reagent for 10 min at 25 °C. After adding in 10 KD Amicon Ultra-0.5 centrifugal filter devices, the protein samples were separated at 13,500 *g* for 20 min, and washed three times with 100 mm^3 of dissolution buffer each time. The samples in filter devices were digested by 50 mm^3 of trypsin at 4% w/w 12 h at 37 °C. Proteins extracted from cells inoculated in treatment solution without BaP for 1 d were digested as the control samples.

2.7. ITRAQ labeling and desalination

Tryptic peptides were labeled with iTRAQ reagent according to the manufacturer's instructions. Briefly, the peptides of the control and experimental samples were labeled with tags 114 and 115, respectively. Ethanol at 150 mm^3 was added to each tube of iTRAQ reagent. After the tryptic peptides were transferred to a new tube, chromatographic-grade water at 100 mm^3 was added to stop the reaction. Subsequently, the iTRAQ-labeled samples were mixed, vortexed, span, desalinated with Strata-X (Phenomenex, USA), and separated by strong cation exchange chromatography, respectively. The labeled peptides were dried in a vacuum concentrator. The samples were then resolved with solution (2% v/v acetonitrile, 0.1% v/v formicacid), centrifuged at 13,500*g* for 20 min, and detected by an AB Sciex Triple-TOF 5600 mass spectrometer (AB Sciex, Framingham, MA, USA) equipped with a Nanospray III source (AB Sciex). A biological replicate per each sample was employed for labeling.

2.8. Protein identification and bioinformatics

Protein identification and relative iTRAQ quantification were performed with UniProt Database and ProteinPilot™ Software 4.5 (AB SCIEX). For iTRAQ quantification, peptides were automatically selected by the Pro Group TM algorithm to calculate the reporter peak area, error factor and *p* value. A reverse database search strategy was adopted to estimate the fault occurrence rate for peptide identification. All the reviewed (263) and unreviewed (28608) protein sequences from *B. brevis* (strains 47, JCM 6285, NBRC 100599, X23) were downloaded (June 5, 2018) at Uniprot (https://www.uniprot.org) as references for protein searching and identification. Identified proteins with at least two matched peptides higher than 95% confidence and a value of false discovery rate lower than 1% were used to quantify protein relative abundance. Subsequently, proteins extracted from cells after BaP degradation with at least a 1.2-fold change in concentration compared to these control samples were identified as the proteins with differential relative abundance. Metabolic pathways catalyzed by these proteins were clarified using the Kyoto Encyclopedia of Genes and Genomes (http://www.genome.jp/kegg), while the interaction networks were analyzed by using *B. brevis* NBRC 100599 as a reference strain in the STRING database (https://string-db.org/).

3. Results and discussion

3.1. Benzo[a]pyrene degradation

The interaction between BaP and cell wall, and the influence of some key factors on the BaP degradation were investigated. Fig. 1a and Table S1 show that the BaP degradation was significantly affected by the initial pH values. An increasing trend of the efficiency of BaP degradation up to 78% with ascending pH values from 3.0 to 7.0 was observed, whereas, a decreased tendency with pH values from 7.0 to 11.0 was shown (Fig. 1a). During the degradation process, the final pH values of the solutions tended to be neutral. This finding infers that the excess H^+ or OH^- in the solution reacted with cell.

To further reveal the correlation between BaP degradation and pH values of the solution, the interactions among BaP, H_3O^+, OH^- and cell wall peptidoglycans were computed. BaP has a tendency to be attracted by tetrapeptides due to their lipophilic properties (Fig. S1a). The excess H_3O^+ in acidic solution tends to be adhered to carboxyl group because of the hydrophilic affinity between them, resulting in the alteration of peptidoglycan structure (Fig. S1b) and the increase in pH values. The reaction occurs between carboxyl group and excess OH^- in the alkaline solution resulting in the decrease in pH values. This finding is consistent with the alteration of pH values during the BaP degradation process shown in Fig. 1a, and it also indicates that cell wall is the outer barrier keeping the intracellular biomolecules of *B. brevis* from being attacked by exotic chemicals. The coexistence of BaP and H_3O^+/OH^- does not change the interaction between cell wall and BaP (Fig. 1b, Fig. S1c and S1e) because the BaP adsorption, and the reactions between H_3O^+/OH^- and cell wall separately occurred with different effective groups. Consequently, it can be inferred that H_3O^+ or OH^- depresses BaP degradation through triggering the inhibition in cellular metabolism not the competition of binding sites.

Fig. 1c and Table S2 show that with the increase in the initial biomass dosage from 0.1 to 0.3 g dm^{-3}, the efficiency of BaP degradation linearly enhanced, followed by a slow rising phase with further increase in biomass. For the protein content, it does not show a linear upward trend with the increase in biomass. These results indicate that the efficiency of BaP degradation primarily depended on *B. brevis* biomass. When the biomass increased to a certain value, it would trigger nutrient competition, resulting in the apoptosis of some cells. Fig. 1d and Table S3 illustrate that the suitable temperature for BaP degradation, and for Ca/Mg and Na/K ATP activities ranged from 25 °C to 30 °C, indicating the relationship between the BaP degradation and protein activities.

To predict the functional proteins related to BaP degradation, the proteome of *B. brevis* in Uniprot database was annotated. The metabolic reactions and pathways mediated by the functional proteins were mapped in the KEGG database (Fig. S2). The results show that several functional proteins were responsible for enzyme-mediated reactions (Eqs. (1)–(9)) associated with xenobiotics degradation. Some of them catalyzed carboxylysis, producing CO_2. Ring-cleavage extradiol dioxygenase, ring-cleaving dioxygenase and 3-hydroxyanthranilate 3, 4-dioxygenase catalyze the cleavage of aromatic rings (Cai et al., 2017). For 3-hydroxyanthranilate 3, 4-dioxygenase, it can transform 3-hydroxyanthranilate to 2-amino-3-carboxymuconate semialdehyde (Brkic et al., 2015). Ring-cleavage extradiol dioxygenase and ring-cleaving dioxygenase utilize a single catalytic iron to incorporate an atom of dioxygen into a substrate, resulting in the cleavage of carbon-carbon bond in aromatic ring, which is the key step for BaP degradation. The production of 1-naphthol and 2-naphthol (Fig. 1e and Table S4) revealed the oxygenation event initially catalyzed by these mentioned dioxygenase, followed by the carboxylysis mediated by decarboxylase, NAD^+ oxidoreductase, tautomerase and dehydrogenase.

2-Carboxy-2, 5-dihydro-5-oxofuran-2-acetate < = > 2-Oxo-2, 3-dihydrofuran-5-acetate + CO_2 (1)

2-Hydroxymuconate semialdehyde + NAD^+ + H_2O < = > 2-Hydroxymuconate + NADH + H^+ (2)

(Hydroxymethylphenyl) succinyl-CoA + NAD^+ < = > Benzoyl succinyl-CoA + NADH + H^+ (3)

2-Hydroxymuconate semialdehyde + NAD^+ + H_2O < = > 2-Hydroxymuconate + NADH + H^+ (4)

2-Hydroxymuconate < = > gamma-Oxalocrotonate (5)

gamma-Oxalocrotonate < = > 2-Hydroxy-2, 4-pentadienoate + CO_2 (6)

2-Hydroxy-5-methyl-cis, cis-muconicsemialdehyde + NAD^+ + H_2O < = > 2-Hydroxy-5-methyl-cis, cis-muconate + NADH + H^+ (7)

2-Hydroxy-5-methyl-cis, cis-muconate < = > 2-Oxo-5-methyl-cis-muconate (8)

2-Oxo-5-methyl-cis-muconate < = > 2-Hydroxy-cis-hex-2, 4-dienoate + CO_2 (9)

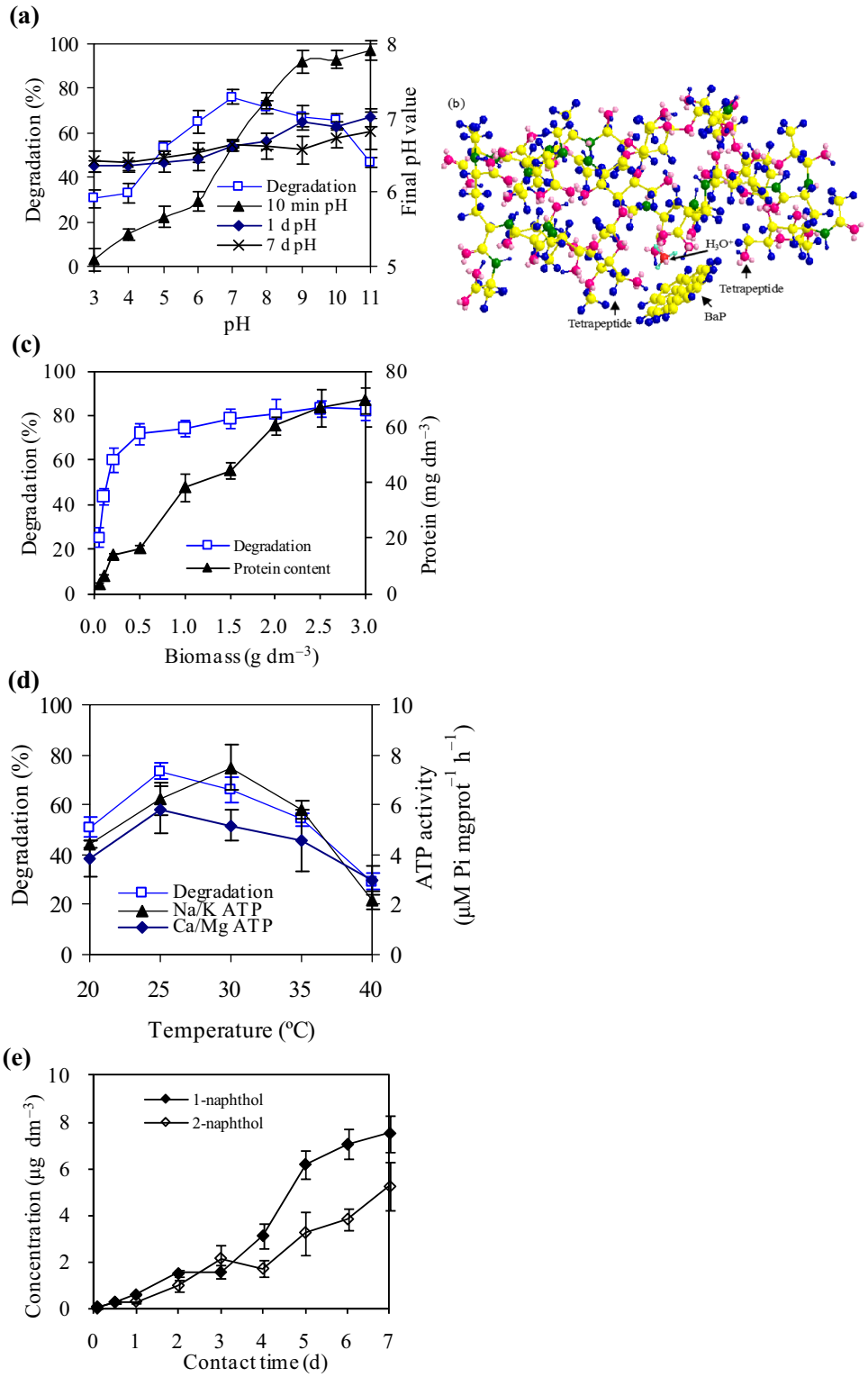

Fig. 1. Effect of initial pH values, biomass and temperature on degradation of 1 mg dm^{-3} BaP by *Brevibacillus brevis*, and the interaction among cell wall, BaP, H_3O^+ and OH^-. (a) Degradation efficiencies and final pH values of solutions; (b) Interaction among cell wall, BaP and H_3O^+; (c) BaP degradation by different biomass; (d) Effect of temperature on BaP degradation, Na^+/K^+–ATPase and Ca^{2+}/Mg^{2+}–ATPase activities; and (e) Concentrations of the produced 1-naphthol and 2-naphthol during the BaP degradation process at 25 °C. Asterisk indicates significant differences between the treated samples and the control samples.

3.2. Benzo[a]pyrene removal, biosorption and bioaccumulation

The BaP removal is calculated by the decrease in BaP concentration in the resultant supernatant after cells were separated by centrifugation. It is attributed to the joint effect of BaP biosorption, accumulation and degradation. Fig. 2a shows that the removal was initially dominated by biosorption because 50.7% of BaP was absorbed by *B. brevis* within 2 h. With the time elongation, the removal was gradually prevailed by degradation. For BaP biosorption, it exhibited a fast declining trend at the first day, followed by a slow downward tendency (Fig. 2a).

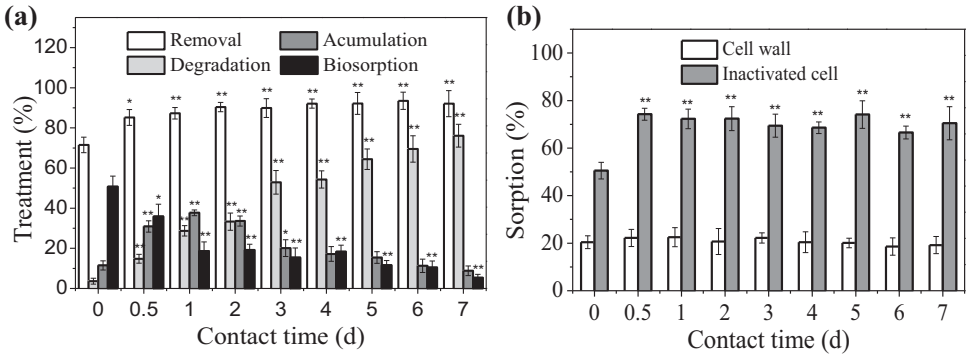

Fig. 2. Biosorption, degradation and accumulation of 1 mg dm^{-3} of BaP by *Brevibacillus brevis* at 25 °C. (a) BaP biosorption, degradation, removal and accumulation by viable cells; and (b) BaP adsorption by the cell wall separated from cells through cell disruption, and by dead cells inactivated by 2% glutaraldehyde for 24 h. Asterisk indicates significant differences between the treated samples and the control samples.

It can be deduced that BaP biosorption is a rapid process, primarily depending on the hydrophobic interactions between BaP and hydrocarbyl constituents of the cell wall and membrane. The decreasing trend means that the absorbed BaP was transported into the cytoplasm.

The peptidoglycan layer of microbial cells is composed of hexagonal units with 30 m^{-10} diameter helical periodicities and 70 m^{-10} diameter pores (Kim et al., 2015). It means that BaP can diffuse across the cell wall because the size of BaP is less than 20 m^{-10}. The increase in BaP accumulation and degradation at the same period of rapid biosorption further confirmed the above deduction. The declining biosorption and accumulation after 1 d was resulted from the degradation of the intracellular BaP (Fig. 2a).

To verify reasons of the decrease in BaP biosorption, BaP adsorption by the cell wall and inactivated cells was performed. The percentage of absorbed BaP by the cell wall during the whole experimental period did not show significant alteration (Fig. 2b). It suggests that BaP binding is a rapid process primarily dependent on the physical interactions between BaP and the cell wall. The efficiencies of BaP adsorption by inactivated cells increased from 51% (2 h) to 74% (0.5 d). These results further confirmed the diffusion of absorbed BaP from the cell wall to the cytoplasm because the removed BaP could not be degraded by inactivated cells.

3.3. Carbon substrate metabolism during benzo[a]pyrene degradation

For the control samples, xylose could not be metabolized (Fig. 3a). With time extension, the enhanced optical density of the solutions with 2-hydroxy benzoate, 4-hydroxy benzoate, phenylalanine and phenylethylamine clarifies that *B. brevis* could utilize compounds with aromatic ring as sole carbon nutrients. It is also an evidence to reveal why this species could degrade polycyclic aromatic hydrocarbons. The ring connected groups, including hydroxyl, carboxyl and amine, did not induce the significant difference into the use of these compounds.

For carbohydrate, polysaccharide glycogen and phosphorylated monosaccharide glucose-1-phosphate were difficult to be degraded when compared to disaccharides (lactose and cellobiose) and glucoside (beta-methyl-D-glucoside). After glycogen phosphorylase catalyzes the phosphorolytic cleavage of a glucosyl residue from a glycogen polymer, the produced glucose has a phosphate group on its C1. Subsequently, phosphoglucomutase transfers the phosphate group to C6 (Stitt and Zeeman, 2012), resulting in the generation of glucose 6-phosphate, which is the most common form of glucose entering a cell. These findings confirm that both the phosphorylation of glycogen and the transport of glucose 1-phosphate into *B. brevis* were speed-limiting steps for carbohydrate metabolism.

The degradation of amino acids often involves deamination by moving its amino group to α-ketoglutarate, forming glutamate. After the removal of an amino group, the remainder of the molecule can be used to synthesize new amino acids, or it can be used for energy metabolism by entering the metabolic pathway of glycolysis or citrate cycle (Wan et al., 2015). As a sole carbon nutrient, each amino acid selected in the current study was easily used by cells. The above results mean that carbon metabolism by *B. brevis* was primarily depended on the molecular structure of these substrates.

The metabolism of galactonic acid lactone, arginine, pyruvate methyl ester, xylose, galacturonic acid, asparagine, phenylalanine, Tween 80, serine, N-acetyl-D-glucosamine, γ-hydroxybutyric acid, threonine, glucosaminic acid, itaconic acid, glycyl-L-glutamic acid, cellobiose, ketobutyric acid, phenylethylamine, lactose, glycerol, malic acid and putrescine after the BaP degradation was upregulated while the use of Tween 40 and glycogen was downregulated. These results mean that the metabolic pathways of the central carbohydrate metabolism, amino acid metabolism, fatty acid metabolism and aromatics degradation were accelerated for the BaP degradation (Fig. 3b).

Compared with the control cells, an insightful finding of carbon substrate metabolism is that xylose could be used, whereas, α-cyclodextrin could no longer be metabolized by cells after the BaP degradation. Xylose in prokaryotes typically metabolizes via an isomerase pathway and two oxidative pathways. In the isomerase pathway, xylose isomerase converts xylose into xylulose. In the oxidative pathway, xylose is oxidized to xylono-lactone by a xylose dehydrogenase followed by the formation of xylonic acid via lactonase hydrolysis. A xylonate dehydratase is splitting off a water molecule resulting in 2-keto-3-deoxy-xylonate, which can be split by an aldolase to pyruvate and glycolaldehyde (Cabulong et al., 2017), or transformed by dehydratase forming 2-ketoglutarate (Radek et al., 2014).

The fact that the control cells did not use xylose means that xylose isomerase was an induced enzyme. BaP was an inductive agent for its expression. That is why xylose could be used by cells after the BaP degradation.

Both glycogen and α-cyclodextrin are polysaccharides of glucose linked by α-1, 4 glycosidic bonds. To transport and use these extracellular polymers, cells need to release α-amylase and glycogen phosphorylase to cleave the α-1, 4 linkages (Moore et al., 2015). Fig. 3b confirms that BaP could silence the expression of glucoamylase and glycogen phosphorylase for the cleavage of α-1, 4 linkages because these cells did not metabolize glycogen and α-cyclodextrin after the BaP degradation.

3.4. Organic acid release during benzo[a]pyrene degradation

All the detected organic acids showed an elevated trend at the initial days during the process of BaP degradation (Fig. 4a), which indicates their upregulated biosynthesis or the increased release induced by the stress of BaP and its generated intermediates. The following downward tendency confirms that a portion of the released organic acids was metabolized by cells.

Lactic acid, acetic acid and oxalic acid are the important intermediates produced in the metabolic pathways of pyruvate metabolism and citrate cycle (Fig. 4b). Several pathways exist for the enzyme-mediated conversion of oxalic acid. It can be generated through the dehydrogenation of pyruvate catalyzed by lactate dehydrogenase ferrocytochrome c (Eq. (10)) and reduced nicotinamide adenine

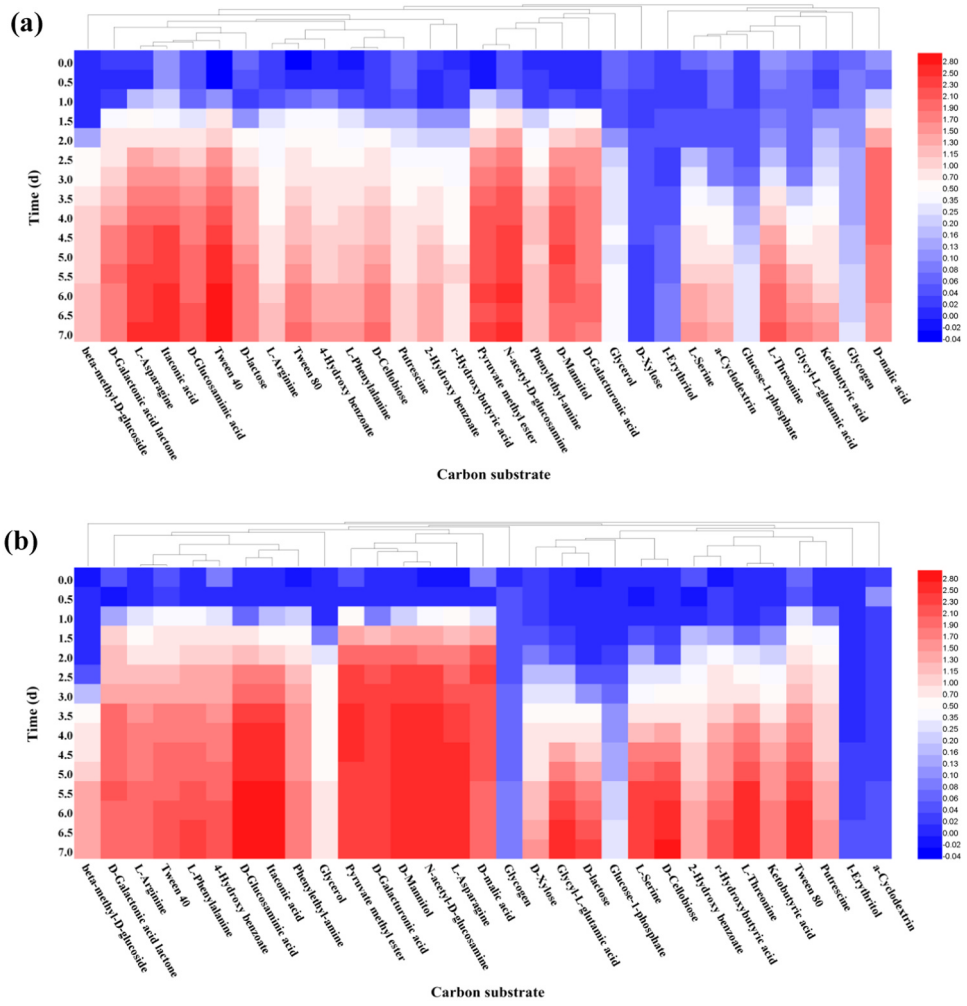

Fig. 3. Cellular metabolic activities in organic carbon use before (a) and after BaP degradation for 7 d (b).

dinucleotide (NADH) (Eq. (11)), or through the transformation of propanoate catalyzed by propanoate-CoA transferase (Eq. (12)), or via the conversion of malate and pyruvate to lactic acid and oxaloacetate (Eq. (13)), which can further hydrolyzed to oxalic acid and acetic acid mediated by oxaloacetate oxidoreductase, or from oxidoreduction by NAD^+ oxidoreductase (Eq. (14)) (Reichardt et al., 2014). For acetic acid, it is primarily converted by acetyl-CoA hydrolase (Eqs. 15–18) (Horibata et al., 2013). At least there are two pathways for the biotransformation of oxalate (Kumar et al., 2016). It can be converted to formate or glyoxylate (Eq. (19)), which is an intermediate connected the transformation of succinate, isocitrate and malate.

The extracellular concentrations of these organic acids exhibited the same upward tendency clarify that the pathways of pyruvate metabolism and citrate cycle were upregulated in the initial days.

$$\text{Pyruvate} + 2\ \text{Ferrocytochrome c} + 2H^+ <=> \text{Lactate} + 2\ \text{Ferricytochromec} \quad (10)$$

$$\text{Pyruvate} + \text{NADH} + H^+ <=> \text{Lactate} + NAD^+ \quad (11)$$

$$\text{Propanoate} + \text{Lactoyl-CoA} <=> \text{Lactate} + \text{Propanoyl-CoA} \quad (12)$$

$$\text{Malate} + \text{Pyruvate} <=> \text{Lactate} + \text{Oxaloacetate} \quad (13)$$

$$\text{Lactaldehyde} + NAD^+ + H_2O <=> \text{Lactate} + \text{NADH} + H^+ \quad (14)$$

$$\text{ADP} + \text{Acetyl phosphate} <=> \text{ATP} + \text{Acetate} \quad (15)$$

$$\text{Orthophosphate} + \text{Acetyl phosphate} <=> \text{Diphosphate} + \text{Acetate} \quad (16)$$

$$\text{AMP} + \text{Diphosphate} + \text{Acetyl-CoA} <=> \text{ATP} + \text{Acetate} + \text{CoA} \quad (17)$$

$$\text{ADP} + \text{Acetyl-CoA} + \text{Orthophosphate} <=> \text{ATP} + \text{Acetate} + \text{CoA} \quad (18)$$

$$\text{Glyoxylate} + H_2O + O_2 <=> \text{Oxalate} + H_2O_2 \quad (19)$$

3.5. Ion transport and ATPase activities

K^+ began with increased intake in the first 3 days, and ended with release. Na^+ showed a release tendency during the BaP degradation period while PO_4^{3-} was used by cells (Fig. 5a). During the degradation process, energy is needed to degrade BaP, and to regulate the related metabolic reactions (Eqs. (1)–(19)); hence, ATP and other P-containing polymers, which need PO_4^{3-} as a phosphorus source, are consumed quickly. The fact that the activities of Na^+/K^+-ATPase and Ca^{2+}/Mg^{2+}-ATPase enhanced during the degradation process compared to the initial time was the direct evidence to clarify PO_4^{3-} consumption.

According to the annotation of functional proteins related to ion transport in the Database of Integrated Microbial Genomes & Microbiomes (https://img.jgi.doe.gov/), two Na^+ transporter (NatA and NatB), three K^+ transporters (KdpA, KdpB and KdpC), and six PO_4^{3-} transporters expressed in *B. brevis* were responsible for Na^+, K^+ and PO_4^{3-} transport and efflux (Table S5). The concentrations of extracellular ions detected in the current study confirm that the regulation of

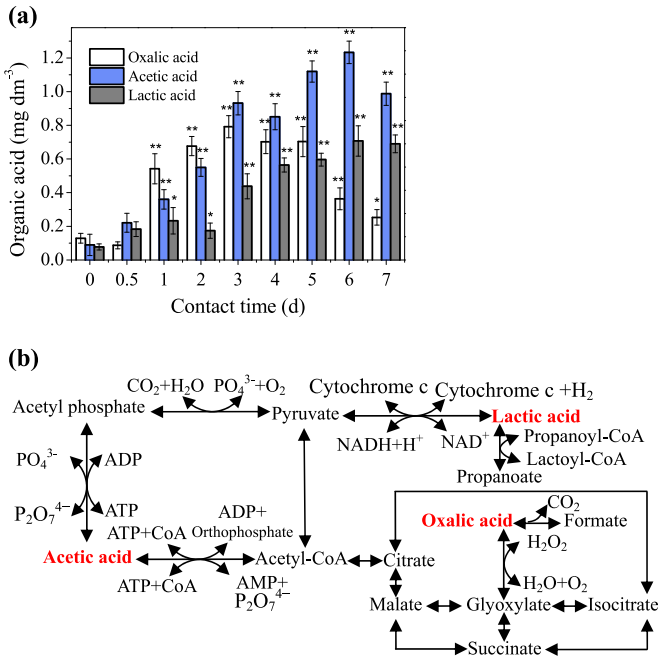

Fig. 4. Organic acid release by *Brevibacillus brevis* at 25 °C during BaP degradation. (a) The release of lactic acid, acetic acid and oxalic acid; and (b) The metabolism pathways of lactic acid, acetic acid and oxalic acid. Asterisk indicates significant differences between the treated samples and the control samples.

these proteins in the BaP degradation process exhibited different tendencies of expression. For Na^+ extrusion, NatA and NatB were upregulated in the first five days, whereas, the expression of KdpA, KdpB and KdpC performed an opposite trend. In the process of BaP degradation, proteins associated with PO_4^{3-} transport were activated for PO_4^{3-} metabolism.

3.6. Metabolic and proteomic mechanism

After the BaP degradation, the relative abundance of 43 proteins was significantly increased, whereas, the abundance of 13 proteins was decreased (Table 1). These upregulated proteins primarily catalyzed pyruvate metabolism, citrate cycle, amino acid metabolism, purine metabolism, ribosome metabolism, energy metabolism and protein synthesis (Fig. 6a). The interactions of the differentially abundant proteins also enriched in the same pathways (Fig. 6b). These findings are consistent with the upward regulation of carbohydrate metabolism, amino acid metabolism, fatty acid metabolism, aromatics degradation (Fig. 3), pyruvate metabolism and citrate cycle (Fig. 4b) in the above experiments.

The increased relative abundance of pyruvate dehydrogenase E1 component subunit beta (PdhB) and cell wall protein precursor (BBR47) accelerated the transformation of pyruvate to acetyl-CoA by catalyzing the metabolites generated in glycolysis (Takenaka et al., 2017), which confirmed the increase in cellular carbohydrate consumption during the BaP degradation. That is why the metabolism of most of the extracellular carbon substrates was upregulated (Fig. 3). Acetyl-CoA derived from pyruvate oxidation was subsequently conveyed the carbon atoms in the acetyl group to the citrate cycle for the generation of energy and precursors of NADH and amino acids. Through the catalysis of isocitrate dehydrogenase (Icd), succinyl-CoA ligase [ADP-forming] subunit beta (SucC), probable malate: quinone oxidoreductase (Mqo) and NAD-dependent malic enzyme (YtsJ), some organic acids such as glutarate and oxaloacetate were derived from acetyl-CoA, providing precursors of alanine, aspartate, glutamate, valine and isoleucine for protein synthesis (Ishihara et al., 2015). In the amino acid metabolism process, two groups of enzymes dihydroxy-acid dehydratase (IlvC and IlvD) and ornithine aminotransferase (RocA and RocD) were responsible for the conversion of substrates to products via dehydration reactions (Titov et al., 2016).

Among the generated amino acids in the current study, aspartate and glutamate were combined with carbon and nitrogen atoms from other intermediates to form purine that was used as the bases in guanosine triphosphate (GTP), guanosine diphosphate (GDP), guanosine monophosphate (GMP), xanthosine 5′-phosphate (XMP), inosine monophosphate (IMP), adenosine 5′-monophosphate (AMP), adenosine 5′-diphosphate (ADP), adenosine 5′-triphosphate (ATP), ribonucleic acid (RNA) and deoxyribonucleic acid (DNA). DNA-directed RNA polymerase subunit beta (RopB), nucleoside diphosphate kinase (Ndk), adenylosuccinate synthetase (PurA) and guanylate kinase (Gmk) were the key note enzymes regulating the transformation among these compounds. The upexpressed mRNA carried genetic information from DNA to the small ribosomal subunits, 30S ribosomal protein S5 (RpsE), 30S ribosomal protein S6 (RpsF), 30S ribosomal protein S7 (RpsG), 30S ribosomal protein S8 (RpsH) and 30S ribosomal protein S9 (RpsI), transferring the information to the large subunits, 50S ribosomal protein L1 (RplA), 50S ribosomal protein L7/L12 (RplL), 50S ribosomal protein L15 (RplO), 50S ribosomal protein L21 (RplU) and 50S ribosomal protein L24 (RplX), which are responsible for linking amino acids delivered by transfer RNA to form proteins. This finding is in agreement with the results that the relative abundance of a large proportion of detected proteins was increased during the BaP degradation process.

In the pathways of pyruvate metabolism and citrate cycle, flavin adenine dinucleotide was transformed to its reduced compound, while oxidized NAD^+ was converted to NADH (Titov et al., 2016). These products were used by the oxidative phosphorylation pathway,

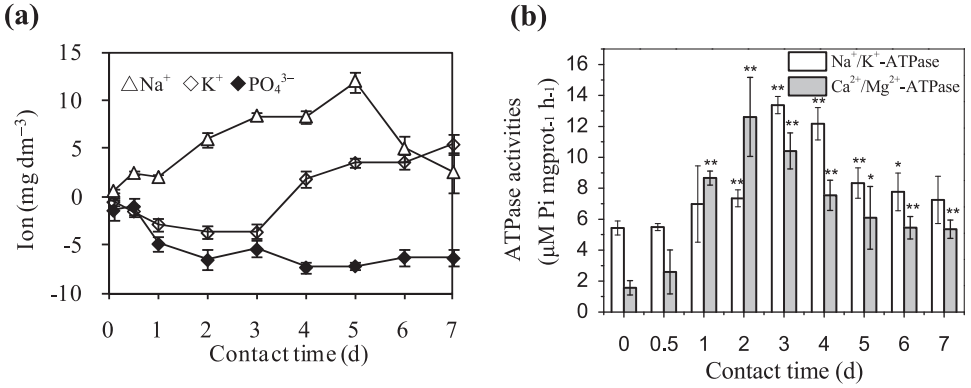

Fig. 5. Ion transport, and Na^+/K^+–ATPase and Ca^{2+}/Mg^{2+}–ATPase activities during BaP degradation. (a) Ion release and use; and (b) Na^+/K^+–ATPase and Ca^{2+}/Mg^{2+}–ATPase activities. Asterisk indicates significant differences between the treated samples and the control samples.

Table 1
The differentially abundant proteins of *Brevibacillus brevis* after BaP degradation.

Number	Unused	% Cov	Accession number	Protein name	Gene name	Peptides(95%)	Degradation intermediates/BaP
1	10.74	35.2	A7GK09	50S ribosomal protein L1	rplA	5	1.330
2	2.01	23.5	B1HMZ8	50S ribosomal protein L7/L12	rplL	2	3.076
3	2.2	19.9	Q5WLP3	50S ribosomal protein L15	rplO	1	16.935
4	3.52	33.3	B1HVB6	50S ribosomal protein L21	rplU	2	4.491
5	2	13.6	A8F996	50S ribosomal protein L24	rplX	1	1.419
6	4.08	22.8	B1HMW3	30S ribosomal protein S5	rpsE	2	2.489
7	2.28	20	Q9K5N8	30S ribosomal protein S6	rpsF	2	27.982
8	2.41	30.1	P22744	30S ribosomal protein S7	rpsG	1	4.169
9	3.41	31.8	Q65P93	30S ribosomal protein S8	rpsH	2	1.259
10	2.47	27.7	Q9KGD4	30S ribosomal protein S9	rpsI	2	1.330
11	10.42	15.1	Q81J48	DNA-directed RNA polymerase subunit beta	rpoB	5	1.803
12	3.17	22.2	P0A3H2	DNA-binding protein HU	hup	2	12.966
13	2.08	30.6	Q5WLN9	Translation initiation factor IF-1	infA	1	1.306
14	4.27	10.2	A7GRE3	Translation initiation factor IF-2	infB	2	1.660
15	7.08	16.8	Q65PB0	Elongation factor G	fusA	5	4.444
16	4.81	14.4	Q9K9T7	Cell division protein FtsZ	ftsZ	2	1.213
17	2	6.1	Q9KCB9	Nucleoside diphosphate kinase	ndk	1	2.582
18	64.35	48.7	P06546	Middle cell wall protein	BBR47_54160	42	3.106
19	23.68	44.9	Q8RU00	60 kDa chaperonin	groL	13	1.941
20	6.23	16	Q9K8F4	ATP-dependent Clp protease ATP-binding subunit	clpX	3	1.459
21	2.05	24.7	P42006	ATP synthase subunit beta	atpD	7	1.923
22	3.03	19.6	Q9K6H4	ATP synthase gamma chain	atpG	1	1.247
23	10.03	26.2	P39126	Isocitrate dehydrogenase [NADP]	icd	4	2.355
24	3.01	23.3	Q65JP0	Succinyl-CoA ligase [ADP-forming] subunit beta	sucC	6	1.318
25	4	10.5	P21874	Pyruvate dehydrogenase E1 component subunit beta	pdhB	2	1.820
26	2.32	7.5	B1HNU2	Probable malate: quinone oxidoreductase	mqo	2	1.871
27	6.16	18	P50735	Cryptic catabolic NAD-specific glutamate dehydrogenase	gudB	3	1.271
28	3.28	12	O34962	Probable NAD-dependent malic enzyme 4	ytsJ	2	1.556
29	10.4	21.2	Q9LCQ5	Chaperone protein	dnaK	6	2.377
30	6.89	56.1	P39158	Cold shock protein	cspC	3	4.335
31	3.56	11.2	P39912	Protein AroA(G)	aroA	2	1.214
32	3.03	19	A7GRA9	Protein RecA	recA	2	2.655
33	3.47	14.4	C1AH22	Adenosylhomocysteinase	ahcY	1	2.355
34	2.72	9.3	A7GKJ4	1-pyrroline-5-carboxylate dehydrogenase	rocA	1	1.657
35	2.42	11.3	P23722	Glyceraldehyde-3-phosphate dehydrogenase	gap	1	1.225
36	2.13	10.5	Q65CR5	Adenylosuccinate synthetase	purA	2	2.355
37	2	7	Q5WEM9	Dihydroxy-acid dehydratase	ilvD	1	1.368
38	2	17.6	Q5WFK3	Guanylate kinase	gmk	1	1.330
39	2	4	Q81VG0	DEAD-box ATP-dependent RNA helicase	cshA	1	3.664
40	2	12	O33114	Ketol-acid reductoisomerase	ilvC	1	65.261
41	2	5.4	B1HS47	Serine–tRNA ligase	serS	2	2.884
42	2	17.7	P08874	Transition state regulatory protein	abrB	1	1.247
43	2	8	Q9K5Z2	Ornithine aminotransferase	rocD	2	1.271
44	2	20.8	Q5WLN4	50S ribosomal protein L17	rplQ	1	0.316
45	2.05	16.8	Q9K869	50S ribosomal protein L20	rplT	1	0.692
46	2.01	25.3	Q5WLP5	30S ribosomal protein S5	rpsE	1	0.809
47	13.3	22.2	P12698	ATP synthase subunit beta	atpD	7	0.249
48	4.25	11.2	B7IQW0	ATP synthase subunit alpha	atpA	2	0.759
49	3.69	19.5	B1HMZ0	Elongation factor Tu	tuf	11	0.794
50	2.07	6.5	Q5WHE8	UPF0365 protein ABC1672	ABC1672	1	0.673
51	2.07	9.7	A7Z0Q9	Adenylate kinase	adk	1	0.631
52	2	5.9	Q8L2I5	Proline dehydrogenase 2		1	0.738
53	2	9.8	A7GTE2	Glutamate-1-semialdehyde 2,1-aminomutase 2	hemL2	1	0.685
54	2	4.4	Q5WEN8	Trigger factor	tig	1	0.449
55	2	15.6	O31818	UPF0291 protein YnzC	ynzC	1	0.441
56	2	5.7	Q9ZBL0	Phosphomethylpyrimidine synthase	thiC	1	0.219

Note: Unused is a score of the quantification for each protein in ProteinPilot software. % Cov is defined as the ratio of the protein sequence covered by the matched peptides. Peptides (95%) indicate the total number of detected peptides (with 95% confidence) for the individual protein. The false discovery rate value of each protein is 0%.

transferring electrons and generating chemical energy in the form of GTP and ATP, which is consistent with the enhanced transformation of GTP and ATP in the purine metabolism pathway in the current study.

4. Conclusions

B. brevis effectively degraded BaP with the production of 1-naphthol and 2-naphthol. During this process, metabolism of galactonic acid lactone, arginine, pyruvate methyl ester, xylose, galacturonic acid, asparagine, phenylalanine, Tween 80, serine, N-acetyl-D-glucosamine, γ-hydroxybutyric acid, threonine, glucosaminic acid, itaconic acid, glycyl-L-glutamic acid, cellobiose, ketobutyric acid, phenylethylamine, lactose, glycerol, malic acid, putrescine, lactic acid, acetic acid, oxalic acid and PO_4^{3-} was upregulated. The insightful finding is that BaP induced the relative abundance of xylose isomerase for xylose metabolism, and inhibited α-cyclodextrin metabolism.

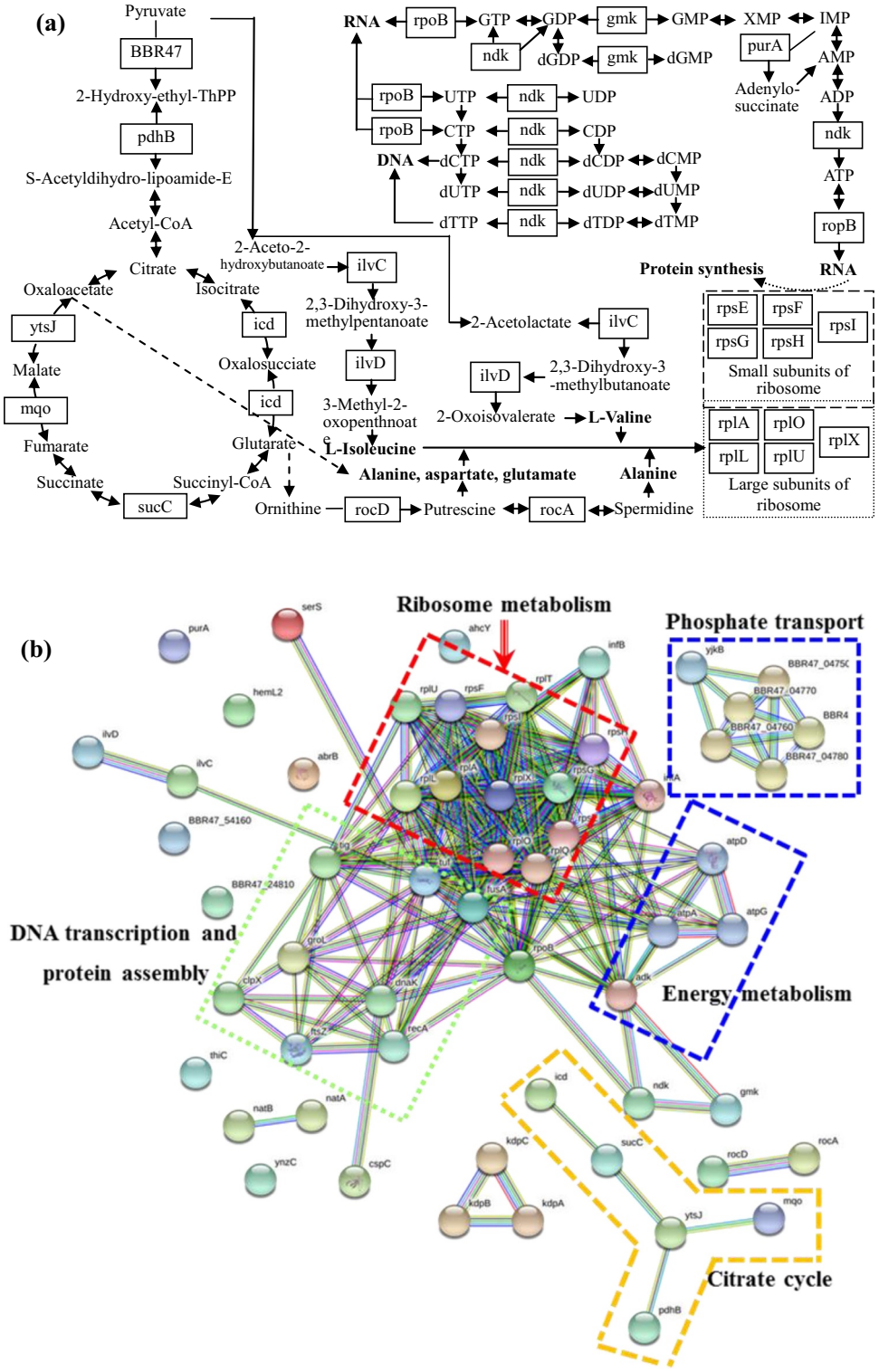

Fig. 6. (a) Metabolic networks catalyzed by the upregulated proteins related to BaP degradation; and (b) Interaction among differentially expressed proteins after BaP degradation.

Acknowledgments

The authors would like to thank the National Key Research and Development Program of China (Nos. 2018YFC1803304, 2017YFD0801300), the Science and Technology Project of Guangdong Province (No. 2016B02024007), the Foundation of Technology Research Center for Petrochemical Resources Clean Utilization of Guangdong Province (No. 201516B10), and the Fundamental Research Funds for the Central Universities (No. 21617453) for their financial support.

Appendix A. Supplementary material

Supplementary data associated with this article can be found in the online version at doi:10.1016/j.ecoenv.2019.01.044

References

Brkic, H., et al., 2015. Human 3-hydroxyanthranilate 3,4-dioxygenase (3HAO) dynamics and reaction, a multilevel computational study. Mol. Biosyst. 11, 898–907.

Cabulong, R.B., et al., 2017. Enhanced yield of ethylene glycol production from D-xylose by pathway optimization in *Escherichia coli*. Enzym. Microb. Technol. 97, 11–20.

Cai, S., et al., 2017. Degradation of diphenyl ether in *Sphingobium phenoxybenzoativorans* SC_ 3 is initiated by a novel ring cleavage dioxygenase. Appl. Environ. Microb. 83. https://doi.org/10.1128/AEM.00104-17.

Chang, Z., et al., 2014. Functional expression of *Carassius auratus* cytochrome P4501A in a novel *Shewanella oneidensis* expression system and application for the degradation of benzo[a]pyrene. J. Biotechnol. 179, 1–7.

Chen, H., et al., 2018. Tissue-specific metabolic responses of the pearl oyster *Pinctada martensii* exposed to benzo[a]pyrene. Mar. Pollut. Bull. 131, 17–21.

Chen, S., et al., 2013. Effect of copper(II) on biodegradation of benzo[a]pyrene by *Stenotrophomonas maltophilia*. Chemosphere 90, 1811–1820.

Fanali, L.Z., et al., 2018. Effects of benzo[a]pyrene on the blood and liver of *Physalaemus cuvieri* and *Leptodactylus fuscus* (Anura: leptodactylidae). Environ. Pollut. 237, 93–102.

Hadibarata, T., Kristanti, R.A., 2012. Fate and cometabolic degradation of benzo[a] pyrene by white-rot fungus *Armillaria* sp. F022. Bioresour. Technol. 107, 314–318.

Horibata, Y., et al., 2013. Enzymatic and transcriptional regulation of the cytoplasmic acetyl-CoA hydrolase ACOT12. J. Lipid Res. 54, 2049–2059.

Ishihara, H., et al., 2015. Quantifying protein synthesis and degradation in arabidopsis by dynamic (CO_2)-C-13 labeling and analysis of enrichment in individual amino acids in their free pools and in protein. Plant Physiol. 168, 74–93.

Kim, M.N., Yoon, M.G., 2010. Isolation of strains degrading poly(Vinyl alcohol) at high temperatures and their biodegradation ability. Polym. Degrad. Stabil. 95, 89–93.

Kim, R.O., et al., 2013. Expression pattern of entire cytochrome P450 genes and response of defensomes in the benzo[a]pyrene-exposed monogonont rotifer *Brachionus koreanus*. Environ. Sci. Technol. 47, 13804–13812.

Kim, S.J., et al., 2015. Peptidoglycan architecture of Gram-positive bacteria by solid-state NMR. BBA–Biomembranes 1848, 350–362.

Kjeldal, H., et al., 2016. Genomic, proteomic, and metabolite characterization of gemfibrozil-degrading organism *Bacillus* sp. GeD10. Environ. Sci. Technol. 50, 744–755.

Krais, A.M., et al., 2016. The impact of p53 on DNA damage and metabolic activation of the environmental carcinogen benzo[a]pyrene: effects in *Trp53(+/+)*, *Trp53(+/-)* and *Trp53(-/-)* mice. Arch. Toxicol. 90, 839–851.

Kumar, V., et al., 2016. Improving nutritional quality and fungal tolerance in soya bean and grass pea by expressing an oxalate decarboxylase. Plant Biotechnol. J. 14, 1394–1405.

Li, C., et al., 2018. Metabolic and proteomic mechanism of bisphenol A degradation by *Bacillus thuringiensis*. Sci. Total Environ. 640, 714–725.

Li, Z.Y., et al., 2016. Complete genome sequence of a benzo[a]pyrene-degrading bacterium *Altererythrobacter epoxidivorans* CGMCC 1.7731T. Mar. Genom. 25, 39–41.

Liao, L., et al., 2015. Biosorption and biodegradation of pyrene by *Brevibacillus brevis* and cellular responses to pyrene treatment. Ecotoxicol. Environ. Saf. 115, 166–173.

Moore, S.A., et al., 2015. Effects of alpha-amylase reaction mechanisms on analysis of resistant-starch contents. Carbohydr. Polym. 115, 465–471.

Pawlowski, A.C., et al., 2016. A diverse intrinsic antibiotic resistome from a cave bacterium. Nat. Commun. 7.

Radek, A., et al., 2014. Engineering of *Corynebacterium glutamicum* for minimized carbon loss during utilization of D-xylose containing substrates. J. Biotechnol. 192, 156–160.

Reichardt, N., et al., 2014. Phylogenetic distribution of three pathways for propionate production within the human gut microbiota. ISME J. 8, 1323–1335.

Shi, Q., et al., 2017. Inflammation and the chemical carcinogen benzo[a]pyrene: partners in crime. Mutat. Res-Rev. Mutat. 774, 12–24.

Shuona, C., et al., 2017. Physiology and bioprocess of single cell of *Stenotrophomonas maltophilia* in bioremediation of co-existed benzo[a]pyrene and copper. J. Hazard. Mater. 321, 9–17.

Song, Z., et al., 2012. Tostadin, a novel antibacterial peptide from an antagonistic microorganism *Brevibacillus brevis* XDH. Bioresour. Technol. 111, 504–506.

Sowada, J., et al., 2014. Degradation of benzo[a]pyrene by bacterial isolates from human skin. FEMS Microbiol. Ecol. 88, 129–139.

Speciale, A., et al., 2018. Experimental exposure of blue mussels (*Mytilus galloprovincialis*) to high levels of benzo[a]pyrene and possible implications for human health. Ecotoxicol. Environ. Saf. 150, 96–103.

Stitt, M., Zeeman, S.C., 2012. Starch turnover: pathways, regulation and role in growth. Curr. Opin. Plant Biol. Biol. 15, 282–292.

Takenaka, M., et al., 2017. Acetyl-CoA production by encapsulated pyruvate ferredoxin oxidoreductase in alginate hydrogels. Bioresour. Technol. 227, 279–285.

Tang, S., et al., 2014. Tea saponin enhanced biodegradation of decabromodiphenyl ether by *Brevibacillus brevis*. Chemosphere 114, 255–261.

Titov, D.V., et al., 2016. Complementation of mitochondrial electron transport chain by manipulation of the NAD^+/NADH ratio. Science 352, 231–235.

Wan, P.J., et al., 2015. Pathways of amino acid degradation in *Nilaparvata lugens* (Stal) with special reference to lysine-ketoglutarate reductase/saccharopine dehydrogenase (LKR/SDH). PLoS One 10.

Wei, K., et al., 2017. Characteristics and proteomic analysis of pyrene degradation by *Brevibacillus brevis* in liquid medium. Chemosphere 178, 80–87.

Ye, J., et al., 2017. Heterogeneous photocatalysis of tris(2-chloroethyl) phosphate by UV/TiO_2: degradation products and impacts on bacterial proteome. Water Res. 124, 29–38.

Ye, J., et al., 2013. Biosorption and biodegradation of triphenyltin by *Brevibacillus brevis*. Bioresour. Technol. 129, 236–241.

Zhang, L., et al., 2017. Exposure to lethal levels of benzo[a]pyrene or cadmium trigger distinct protein expression patterns in earthworms (*Eisenia fetida*). Sci. Total Environ. 595, 733–742.